

Selective On-Surface Reactions of the Alkenyl *gem*-Dibromide Group Directed by Substrate Lattices

Faming Kang, Wenze Gao, Liangliang Cai, Cuiyu Li, Chunxue Yuan, and Wei Xu*

Cite This: *J. Phys. Chem. C* 2021, 125, 23840–23847

Read Online

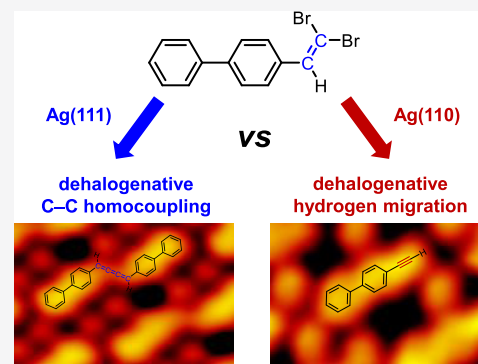
ACCESS |

Metrics & More

Article Recommendations

Supporting Information

ABSTRACT: On-surface synthesis has demonstrated great advantages for atomically precise fabrication of surface-supported nanostructures that could be promising for the next generation of semiconducting materials and molecular electronic devices. The challenging and key issue in this field is to steer surface reaction pathways achieving precise synthesis. The alkenyl *gem*-dibromide group has been shown to have versatile chemical reactivity. Herein, by introducing such a complicated functional group on surfaces, we demonstrate that selective on-surface reactions, that is, homocoupling and hydrogen migration, could be achieved on Ag(111) and Ag(110) surfaces, respectively. The underlying mechanism of lattice-directed selectivity is revealed by extensive density functional theory (DFT) calculations on the competitive reaction pathways. Such a lattice-directed strategy would be an important means for steering on-surface reaction pathways, aiming to achieve atomically precise synthesis with high efficiency and selectivity.



INTRODUCTION

On-surface synthesis has attracted intense research efforts due to its great advantages in the atomically precise fabrication of low-dimensional nanostructures, which are promising for applications in the construction of molecular electronic devices and functional nanomaterials.^{1–3} By developing such a strategy, particularly, various novel carbon nanostructures like graphene nanoribbons,^{4,5} nanoporous graphene,¹ graphyne/graphdiyne nanowires,^{6,7} and organometallic polyynes^{8,9} have been precisely fabricated on surfaces, which allows for further fine characterizations and accurate measurements. On the other hand, on-surface synthesis could provide unique reaction pathways because of surface confinement effects that are distinct from conventional solution chemistry.^{10,11} To date, one of the big challenges in this field is to steer surface reaction pathways achieving precise synthesis with high efficiency and selectivity, and the key issue is to reveal the influencing factors of reaction pathways and their regulation mechanisms. It was previously identified that on-surface reaction pathways could be steered by pre-self-assembled structures,^{12–15} reaction kinetics and thermodynamics,^{8,16} elements and lattices of substrates,^{8,17,18} etc. For example, the terminal alkyne group could undergo a dehydrogenative C–C coupling reaction on a Ag(111) surface, while on Ag(110), dehydrogenative organometallic coupling was achieved.¹⁹ It is therefore of general interest to further develop such a lattice-directed strategy, aiming to achieve selective on-surface reactions with more complicated functional groups.

The alkenyl *gem*-dibromide group, with versatile chemical reactivity, demonstrated that an elimination reaction occurs and yields terminal alkynyl bromides in solution chemistry (as

shown in Scheme 1a),^{20–22} while on metal surfaces (e.g., Au(111), Cu(111), and Cu(110)), sequential dehalogenation followed by C–C homocoupling occurs with the formation of a cumulene moiety.^{23,24}

Moreover, interestingly, on a NaCl surface, sequential dehalogenation followed by skeletal rearrangement preferentially occurs with the formation of an alkyne moiety.²⁵ Herein, by introducing such a complicated alkenyl *gem*-dibromide group on the Ag(111) and Ag(110) surfaces, respectively, from the combination of scanning tunneling microscopy (STM) imaging and density functional theory (DFT) calculations, we demonstrate that selective on-surface reactions directed by substrate lattices are achieved as shown in Scheme 1b. As a result, on Ag(111), sequential dehalogenation followed by C–C homocoupling occurs with the formation of the cumulene moiety, and interestingly, on Ag(110), sequential dehalogenation followed by hydrogen migration preferentially occurs with the formation of terminal alkyne. The underlying mechanism of lattice-directed selective on-surface reactions is revealed by extensive DFT calculations on the competitive reaction pathways. Such a study would extend the on-surface synthesis strategy by not only designing different molecular precursors

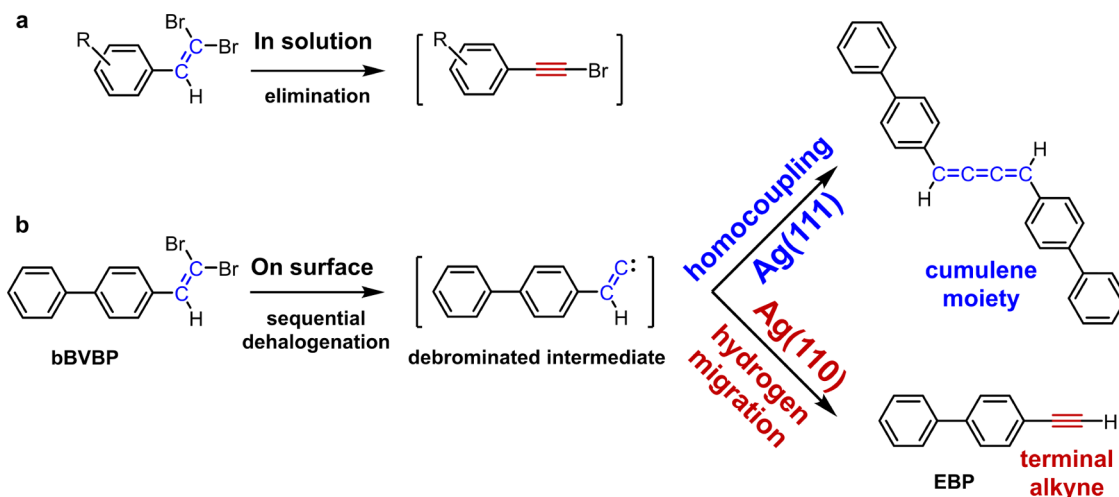
Received: September 10, 2021

Revised: October 13, 2021

Published: October 25, 2021



Scheme 1. (a) Schematic Illustration Showing that the Alkenyl *gem*-Dibromide Group Undergoes an Elimination Reaction Yielding Terminal Alkynyl Bromides in Solution. (b) Schematic Illustration Showing the Different Reaction Pathways of an Alkenyl *gem*-Dibromide (4-(2,2-dibromovinyl)-1,1'-biphenyl, bBVBP) Molecule on Ag(111) and Ag(110). Sequential Dehalogenation of the bBVBP Molecule Leads to the Direct Formation of the Cumulene Moiety via C–C Homocoupling on Ag(111), While on the Ag(110) Surface, Hydrogen Migration of the Debrominated Intermediate Occurs, Which Results in the Formation of a Terminal Alkyne



but also deeply steering surface reaction pathways with high efficiency and selectivity.

EXPERIMENTAL AND THEORETICAL METHODS

The STM experiments were carried out in a ultra-high vacuum (UHV) chamber with a base pressure of 1×10^{-10} mbar. The whole system was equipped with a variable-temperature, fast-scanning “Aarhus-type” STM using electrochemically etched W tips purchased from SPECS,^{26,27} where measurements were carried out at 100–150 K. A molecular evaporator and standard facilities were used for sample preparation. The Ag(111) and Ag(110) substrates were prepared by several cycles of 1.5 keV Ar⁺ sputtering, followed by annealing to 780 K, resulting in clean and flat terraces separated by monatomic steps. After the system was thoroughly degassed, the bBVBP molecules were sublimated from the molecular evaporator onto the substrates. The sample was thereafter transferred within the UHV chamber to the microscope, where measurements were performed in a typical temperature range of 100–150 K, and the typical scanning parameters were $I_t = 0.5$ – 1.0 nA and $V_t = \pm 1000$ – 2000 mV. All of the STM images were further smoothed to eliminate noise.

The calculations were performed in the framework of DFT using a Vienna Ab initio Simulation Package (VASP) code.^{28,29} The projector-augmented-wave method was used to describe the interaction between ions and electrons,^{30,31} and the Perdew–Burke–Ernzerhof generalized gradient approximation of the exchange–correlation functional was employed.³² Van der Waals corrections to the PBE density functional were also included using the DFT-D3 method of Grimme.³³ The atomic structures were relaxed using the conjugate gradient algorithm scheme as implemented in VASP until the forces on all unconstrained atoms were ≤ 0.03 eV/Å for geometry optimization. The simulated STM image was obtained using the Tersoff–Hamann method,³⁴ in which the local density of states (LDOS) is used to approximate the tunneling current. Reaction pathways were calculated with a combination of the climbing image-nudged elastic band (CI-NEB)³⁵ and dimer

methods,³⁶ where CI-NEB was used to find an initial guess of a transition state, which was then refined by the dimer method until the forces acting to the path were converged typically to ≤ 0.03 eV/Å.

RESULTS AND DISCUSSION

After deposition of 4-(2,2-dibromovinyl)-1,1'-biphenyl (bBVBP) molecules on Ag(111) at room temperature (RT, ~ 300 K), we observe the formation of an ordered island structure as shown in Figure 1b. The close-up STM image (Figure 1c) allows identifying that the structure is composed of building blocks with curved shapes (as highlighted by the blue contour). In addition, at the peripheral of ordered islands, another motif with a V shape (as highlighted by the green contour) is also observed (Figure 1d). According to our previous results obtained on the Au(111) and Cu(110) surfaces,^{23,24} combined with a detailed comparison of the experimental topographies and dimensions with the corresponding simulated STM images (Figures 1e and S1) and the calculated adsorption models (Figure 1f,g), it is identified that the reaction products on Ag(111) are dimerized bBVBP molecules with *trans*- or *cis*-cumulene moieties. Such a dehalogenative C–C homocoupling reaction is depicted in Figure 1a. The dot protrusions between the curved motifs are attributed to detached bromine atoms. It should be pointed out that the dehalogenative homocoupling reaction shows a high stereoselectivity on the Ag(111) surface, where a *trans*-cumulene product is a more competitive one with more than 85% on the surface.

On the other hand, we also deposit bBVBP molecules on the Ag(110) surface held at RT, and interestingly, a kind of disordered structure distinct from the reaction products on Ag(111) is obtained (Figure 2b) with a yield of about 70%. It is distinguished that this structure is composed of rod motifs with an implicit tail (as highlighted by the cyan contour) together with dot protrusions attributed to detached bromine atoms. This rod feature indicates that sequential debromination has already occurred at RT but without further C–C

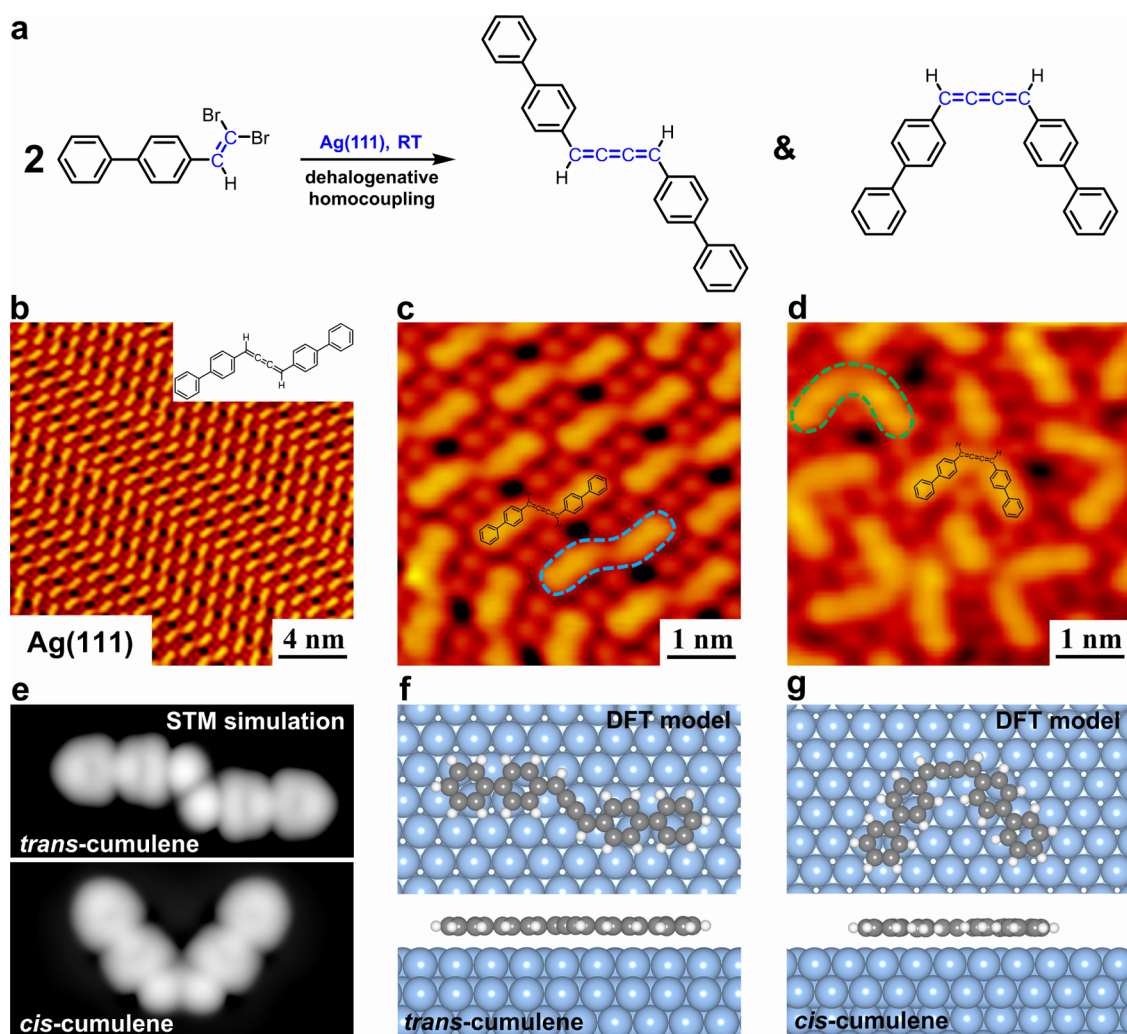


Figure 1. (a) Schematic illustration showing the dehalogenative C–C homocoupling of bBVBP on Ag(111), which leads to the direct formation of *trans*- and *cis*-cumulene moieties. (b) Large-scale and (c) close-up STM images showing the formation of *trans*-cumulene products after deposition of bBVBP molecules on Ag(111) held at ~ 300 K. The STM topography of a *trans*-cumulene product is indicated by the blue contour. (d) Close-up STM image showing the coexistence of *cis*-cumulene products, and one of them is indicated by the green contour. (e) Simulated STM images of *trans*- and *cis*-cumulene products. (f) and (g) DFT relaxed models of *trans*- and *cis*-cumulene products on Ag(111).

coupling. Inspired from the literature,²⁵ sequential dehalogenation of the alkenyl *gem*-dibromide group by atomic manipulation on the NaCl surface leads to a skeletal rearrangement of the debrominated intermediate and consequently results in the formation of the alkyne moiety. Theoretical calculation further demonstrates that a similar process, hydrogen migration, is a barrier-free process in the gas phase (see Figure S2). Based on that, the rod motif observed in Figure 2b is speculated to be alkynyl species [i.e., 4-ethynyl-biphenyl (EBP) molecule shown in Scheme 1b] obtained by hydrogen migration of the debrominated intermediate of bBVBP. To verify our speculation, the ex situ synthesized EBP molecule is chosen as a comparative experiment. As shown in Figure 2c, after deposition of EBP molecules on Ag(110) held at ~ 300 K, the rod motifs of EBP closely resembled the in situ products of bBVBP on Ag(110) at ~ 300 K. Note that the dot protrusions are residual bromine atoms. From this comparative experiment, combined with a detailed comparison of the experimental topographies and dimensions with the corresponding simulated STM image (Figures 2d and S3a), we distinguish that the in situ reaction product of bBVBP on Ag(110) at RT should be the EBP molecule, resulting from

hydrogen migration of the debrominated intermediate of bBVBP.

Next, we anneal the structures shown in Figure 2b at ~ 370 K for about 60 min; it is expected that dehydrogenative organometallic coupling occurs, resulting in the formation of predominant silver-acetylide organometallic products on the surface. A closer examination of the structure (Figure 2e) revealed that the island is composed of an organometallic coupling product as highlighted by the dark blue contour. It is identified that the product structure consists of two lobes at both sides (attributed to the biphenyl groups of EBP molecules) and a dot protrusion in the middle assigned to a silver atom. As the comparative experiment, we also perform the thermal treatment on the structure formed by ex situ EBP molecules. After annealing the structure shown in Figure 2c at ~ 370 K, as expected, we obtained the same silver-acetylide organometallic products (cf. Figure 2f). DFT calculations further reveal the detailed adsorption geometry and the simulated topography of the organometallic species on Ag(110) as shown in Figure 2g. From this comparative experiment, combined with the comparison of the experimental topographies and dimensions with the corresponding

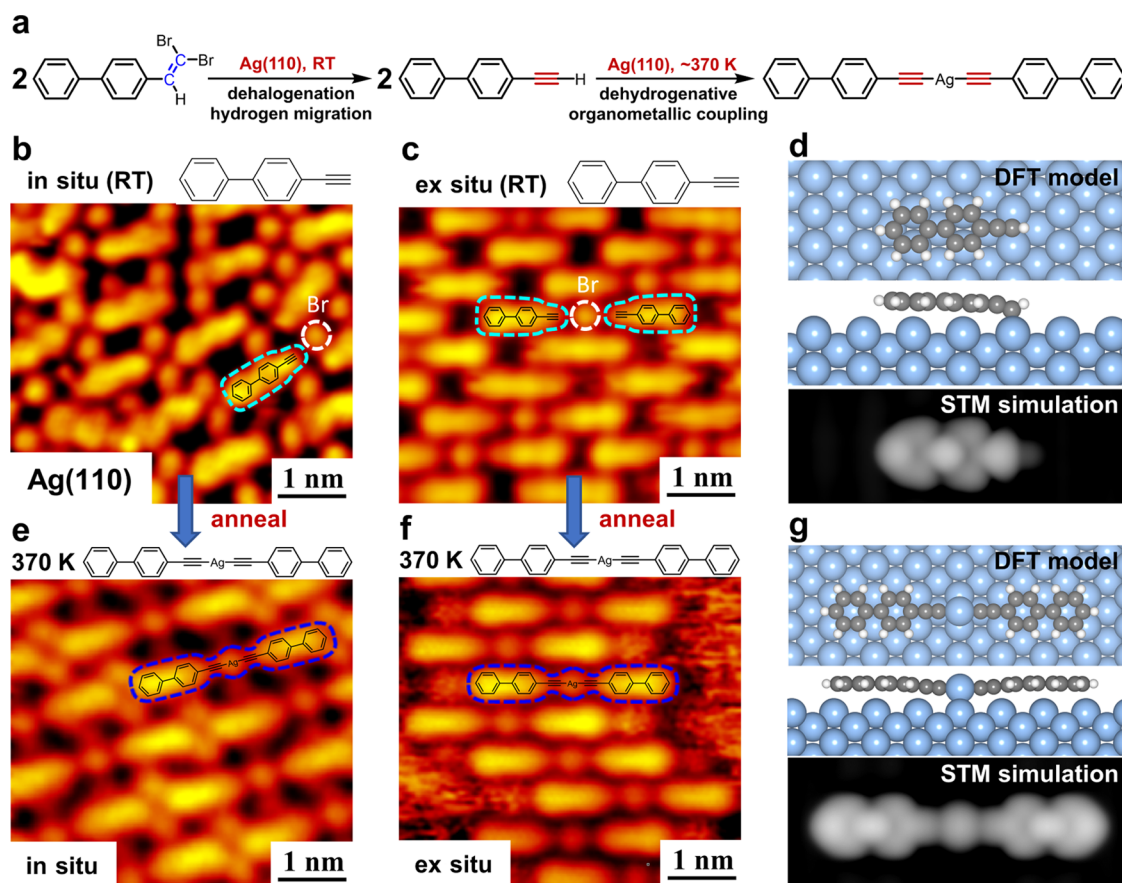


Figure 2. (a) Schematic illustration showing the hydrogen migration after sequential dehalogenation of bBVBP and subsequent dehydrogenative organometallic coupling on Ag(110). (b) STM image showing the in situ formation of the terminal alkynyl product (EBP) through hydrogen migration after sequential dehalogenation of bBVBP on Ag(110) at ~ 300 K. The STM topography of an EBP molecule is indicated by the cyan contour. (c) STM image of the ex situ synthesized EBP molecule adsorbed on Ag(110) in which a single molecule is also indicated by the cyan contour. (d) DFT relaxed models and the simulated STM image of an EBP molecule on Ag(110). (e) and (f) STM images showing the formation of silver-acetylide organometallic products through dehydrogenative organometallic coupling of in situ formed and ex situ synthesized EBP molecules on Ag(110) at ~ 370 K, respectively. The STM topographies of silver-acetylide organometallic species are indicated by the dark blue contours, respectively. (g) DFT relaxed models and the simulated STM image of silver-acetylide organometallic species on Ag(110).

simulated STM image (see Figure S3b), the formation of silver-acetylide organometallic products is confirmed. The whole dehalogenative hydrogen migration and dehydrogenative organometallic coupling reaction are depicted in Figure 2a.

To further compare with the reaction pathway in solution chemistry as shown in Scheme 1a, we have conducted another comparative experiment by employing the 4-bromoethynylbiphenyl (BEBP) molecule, which is the product of the elimination reaction of bBVBP in solution as depicted in Figure 3a. After deposition of BEBP molecules on both the Ag(111) and Ag(110) surfaces held at RT, we observe the direct formation of silver-acetylide organometallic products on both surfaces through debromination of the terminal alkynyl bromide group, followed by organometallic coupling (Figure 3b–d), which is also previously demonstrated on Au(111).^{37–39} The on-surface reaction product of the BEBP molecule is clearly distinct from the products of the bBVBP molecule on both Ag(111) and Ag(110) surfaces at RT, which indicates that the BEBP should not be the reaction intermediate of bBVBP. The occurrence of such an elimination reaction in solution can thus be ruled out for on-surface reactions.

From the above discussion, it is experimentally demonstrated that lattice-directed selective on-surface reactions are

achieved. To further reveal the role of substrate lattices in influencing the reaction pathways, extensive DFT calculations especially on the competitive reaction pathways are performed on the Ag(111) and Ag(110) surfaces. As shown in Figure 4, sequential dehalogenation processes are calculated in the first step, and it is found that the energy barriers of successive C–Br bond activations are 0.66 and 0.50 eV on Ag(111) and 0.22 and 0.27 eV on Ag(110). According to the Arrhenius equation, the dehalogenation processes could occur well below RT. More importantly, competitive reaction pathways, that is, homocoupling vs hydrogen migration, are conducted on Ag(111) and Ag(110). As shown in Figure 5a,b, homocoupling is energetically more favorable than hydrogen migration of debrominated intermediates on Ag(111) (energy barriers are calculated to be 0.26 vs 1.25 eV, respectively), while on Ag(110), shown in Figure 5c,d, hydrogen migration preferentially occurs in comparison with homocoupling (energy barriers are calculated to be 0.65 vs 0.84 eV, respectively). We also consider other possible factors such as kinetics that may affect the reaction pathways. Our DFT calculations show that the debrominated species can diffuse along two of the main directions of the substrate with barriers of 0.17 and 0.19 eV on Ag(111) (Figure S4a), while on the Ag(110) surface, the diffusion barriers are increased to 0.54 and 0.57 eV (Figure

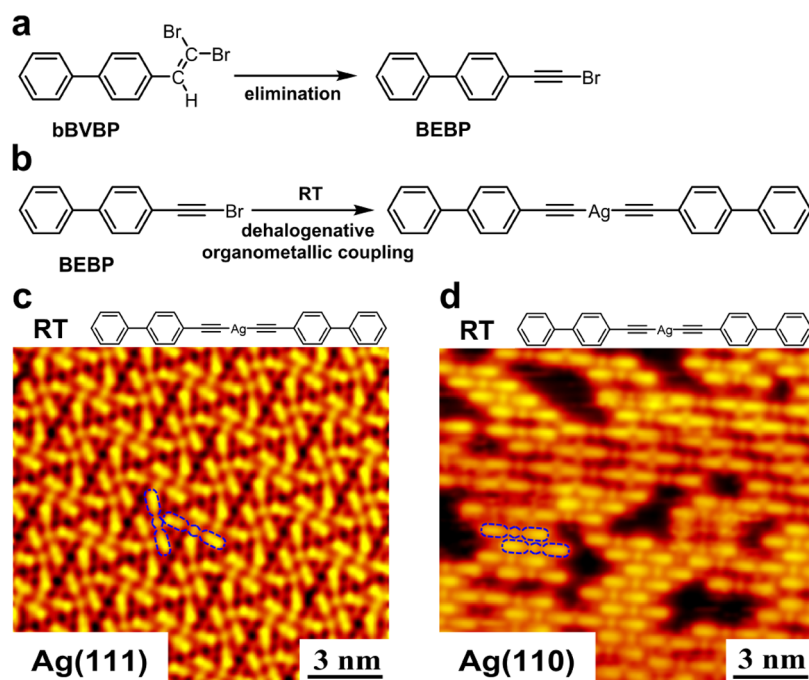


Figure 3. (a) Schematic illustration showing another possible reaction pathway of the alkenyl *gem*-dibromide (bBVBP) molecule, that is, elimination reaction normally occurs in solution, which leads to the formation of terminal alkynyl bromide (BEBP). (b) Schematic illustration and STM images showing the direct formation of silver-acetylide organometallic products after deposition of BEBP molecules on (c) Ag(111) and (d) Ag(110) held at RT.

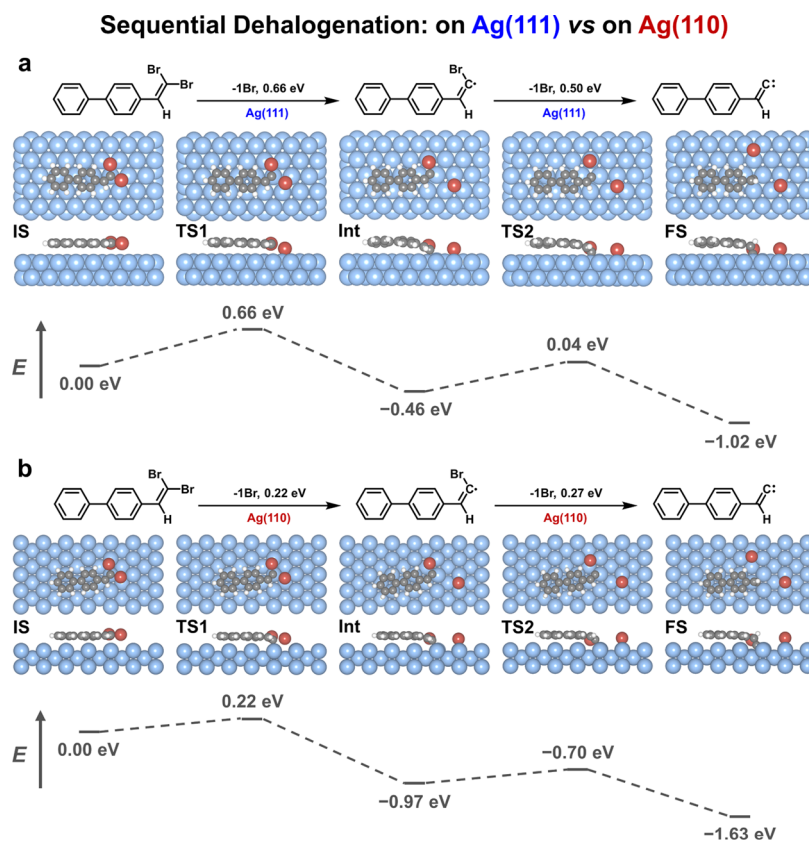


Figure 4. DFT-calculated reaction pathways for the sequential C–Br bond activations of the bBVBP molecule on (a) Ag(111) and (b) Ag(110). The structural models of the initial (IS), transition (TS), intermediate (Int), and final states (FS) along the pathway are also shown.

S4b). These results further illustrate that the Ag(110) surface lattice may significantly hinder the mobility of the absorbed molecules compared with Ag(111), which results in inhibition

of the intermolecular reaction (i.e., homocoupling) and hence gives rise to the intramolecular hydrogen migration. These

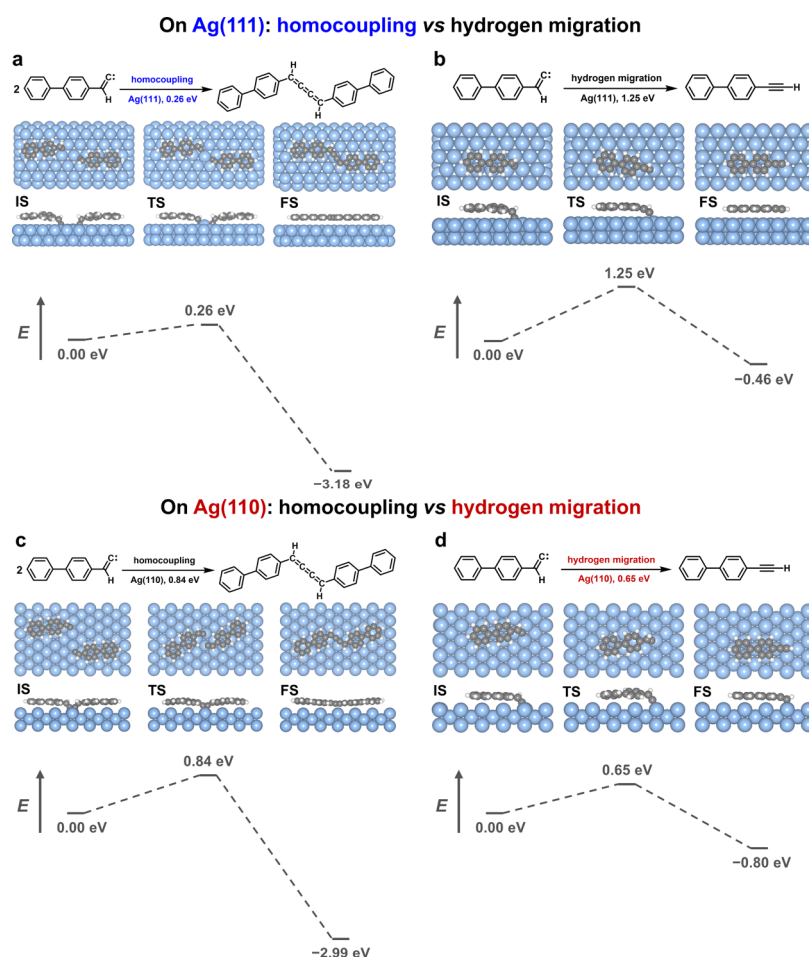


Figure 5. DFT-calculated reaction pathways for homocoupling and hydrogen migration of debrominated intermediates on (a, b) Ag(111) and (c, d) Ag(110), respectively. The structural models of the initial (IS), transition (TS), and final states (FS) along the pathway are also shown.

calculations well account for the experimental observations of selective on-surface reactions steered by substrate lattices.

CONCLUSIONS

In conclusion, from the combination of scanning tunneling microscopy imaging and density functional theory calculations, we demonstrate that selective on-surface reactions, homocoupling and hydrogen migration, in this case, could be achieved by choosing different silver substrate lattices, which is further corroborated by extensive DFT calculations on the competitive reaction pathways. Such a lattice-directed strategy would be an important means for steering on-surface reaction pathways, aiming to achieve atomically precise synthesis with high efficiency and selectivity.

ASSOCIATED CONTENT

Supporting Information

The Supporting Information is available free of charge at <https://pubs.acs.org/doi/10.1021/acs.jpcc.1c08003>.

Detailed comparison of the experimental topology and dimensions with the simulated STM images of cumulene products on Ag(111) and EBP and silver-acetylide organometallic products on Ag(110); DFT-calculated conversion of debrominated intermediate in the gas phase; and DFT-calculated pathways for the diffusion of the debrominated molecules on surfaces (PDF)

AUTHOR INFORMATION

Corresponding Author

Wei Xu – Interdisciplinary Materials Research Center, College of Materials Science and Engineering, Tongji University, Shanghai 201804, P. R. China; orcid.org/0000-0003-0216-794X; Email: xuwei@tongji.edu.cn

Authors

Faming Kang – Interdisciplinary Materials Research Center, College of Materials Science and Engineering, Tongji University, Shanghai 201804, P. R. China

Wenze Gao – Interdisciplinary Materials Research Center, College of Materials Science and Engineering, Tongji University, Shanghai 201804, P. R. China

Liangliang Cai – Interdisciplinary Materials Research Center, College of Materials Science and Engineering, Tongji University, Shanghai 201804, P. R. China

Cuiyu Li – Advanced Computing East China Sub-Center, Suma Technology Co., Ltd., Kunshan 215300, P. R. China

Chunxue Yuan – Interdisciplinary Materials Research Center, College of Materials Science and Engineering, Tongji University, Shanghai 201804, P. R. China

Complete contact information is available at:

<https://pubs.acs.org/doi/10.1021/acs.jpcc.1c08003>

Author Contributions

F.K. and W.G. contributed equally to this work. W.X. conceived and designed the experiments. F.K., W.G., and L.C. performed the STM experiments. F.K. and C.L. did the DFT calculations. C.Y. synthesized the precursor bBVBP. W.X., F.K., and W.G. analyzed the data. W.X. and F.K. drafted the manuscript. All authors proofread, commented on, and approved the final version of the manuscript.

Notes

The authors declare no competing financial interest.

ACKNOWLEDGMENTS

The authors acknowledge the financial support from the National Natural Science Foundation of China (21790351, 22125203).

REFERENCES

- (1) Moreno, C.; Vilas-Varela, M.; Kretz, B.; Garcia-Lekue, A.; Costache, M. V.; Paradinas, M.; Panighel, M.; Ceballos, G.; Valenzuela, S. O.; Peña, D.; et al. Bottom-up Synthesis of Multifunctional Nanoporous Graphene. *Science* **2018**, *360*, 199–203.
- (2) Tsai, H.-Z.; Lischner, J.; Omrani, A. A.; Liou, F.; Aikawa, A. S.; Karrasch, C.; Wickenburg, S.; Riss, A.; Natividad, K. C.; Chen, J.; et al. A Molecular Shift Register Made Using Tunable Charge Patterns in One-Dimensional Molecular Arrays on Graphene. *Nat. Electron.* **2020**, *3*, 598–603.
- (3) Xiang, D.; Wang, X.; Jia, C.; Lee, T.; Guo, X. Molecular-Scale Electronics: From Concept to Function. *Chem. Rev.* **2016**, *116*, 4318–4440.
- (4) Cai, J.; Ruffieux, P.; Jaafar, R.; Bieri, M.; Braun, T.; Blankenburg, S.; Muoth, M.; Seitsonen, A. P.; Saleh, M.; Feng, X.; et al. Atomically Precise Bottom-Up Fabrication of Graphene Nanoribbons. *Nature* **2010**, *466*, 470–473.
- (5) Ruffieux, P.; Wang, S.; Yang, B.; Sánchez-Sánchez, C.; Liu, J.; Dienel, T.; Talirz, L.; Shinde, P.; Pignedoli, C. A.; Passerone, D.; et al. On-Surface Synthesis of Graphene Nanoribbons with Zigzag Edge Topology. *Nature* **2016**, *531*, 489–493.
- (6) Yu, X.; Cai, L.; Bao, M.; Sun, Q.; Ma, H.; Yuan, C.; Xu, W. On-Surface Synthesis of Graphyne Nanowires through Stepwise Reactions. *Chem. Commun.* **2020**, *56*, 1685–1688.
- (7) Wang, T.; Huang, J.; Lv, H.; Fan, Q.; Feng, L.; Tao, Z.; Ju, H.; Wu, X.; Tait, S. L.; Zhu, J. Kinetic Strategies for the Formation of Graphyne Nanowires via Sonogashira Coupling on Ag(111). *J. Am. Chem. Soc.* **2018**, *140*, 13421–13428.
- (8) Sun, Q.; Cai, L.; Wang, S.; Widmer, R.; Ju, H.; Zhu, J.; Li, L.; He, Y.; Ruffieux, P.; Fasel, R.; et al. Bottom-Up Synthesis of Metalated Carbyne. *J. Am. Chem. Soc.* **2016**, *138*, 1106–1109.
- (9) Yu, X.; Li, X.; Lin, H.; Liu, M.; Cai, L.; Qiu, X.; Yang, D.; Fan, X.; Qiu, X.; Xu, W. Bond-Scission-Induced Structural Transformation from Cumulene to Diyne Moiety and Formation of Semiconducting Organometallic Polyynes. *J. Am. Chem. Soc.* **2020**, *142*, 8085–8089.
- (10) Zhong, Q.; Hu, Y.; Niu, K.; Zhang, H.; Yang, B.; Ebeling, D.; Tschakert, J.; Cheng, T.; Schirmeisen, A.; Narita, A.; et al. Benzo-Fused Periacenes or Double Helicenes? Different Cyclodehydrogenation Pathways on Surface and in Solution. *J. Am. Chem. Soc.* **2019**, *141*, 7399–7406.
- (11) Sun, Q.; Cai, L.; Ding, Y.; Xie, L.; Zhang, C.; Tan, Q.; Xu, W. Dehydrogenative Homocoupling of Terminal Alkenes on Copper Surfaces: A Route to Dienes. *Angew. Chem., Int. Ed.* **2015**, *54*, 4549–4552.
- (12) Chen, Q.; Cramer, J. R.; Liu, J.; Jin, X.; Liao, P.; Shao, X.; Gotherf, K. V.; Wu, K. Steering On-Surface Reactions by a Self-Assembly Approach. *Angew. Chem., Int. Ed.* **2017**, *56*, 5026–5030.
- (13) Zhou, X.; Bebensee, F.; Yang, M.; Bebensee, R.; Cheng, F.; He, Y.; Shen, Q.; Shang, J.; Liu, Z.; Besenbacher, F.; et al. Steering Surface Reaction at Specific Sites with Self-Assembly Strategy. *ACS Nano* **2017**, *11*, 9397–9404.
- (14) Zhou, X.; Wang, C.; Zhang, Y.; Cheng, F.; He, Y.; Shen, Q.; Shang, J.; Shao, X.; Ji, W.; Chen, W.; et al. Steering Surface Reaction Dynamics with a Self-Assembly Strategy: Ullmann Coupling on Metal Surfaces. *Angew. Chem., Int. Ed.* **2017**, *56*, 12852–12856.
- (15) Lu, H.; E, W.; Cai, L.; Ma, Z.; Xu, W.; Yang, X. Dissymmetric On-Surface Dehalogenation Reaction Steered by Preformed Self-Assembled Structure. *J. Phys. Chem. Lett.* **2020**, *11*, 1867–1872.
- (16) Wang, S.; Sun, Q.; Gröning, O.; Widmer, R.; Pignedoli, C. A.; Cai, L.; Yu, X.; Yuan, B.; Li, C.; Ju, H.; et al. On-Surface Synthesis and Characterization of Individual Polyacetylene Chains. *Nat. Chem.* **2019**, *11*, 924–930.
- (17) Gao, H.-Y.; Wagner, H.; Zhong, D.; Franke, J.-H.; Studer, A.; Fuchs, H. Glaser Coupling at Metal Surfaces. *Angew. Chem., Int. Ed.* **2013**, *52*, 4024–4028.
- (18) Jiang, L.; Niu, T.; Lu, X.; Dong, H.; Chen, W.; Liu, Y.; Hu, W.; Zhu, D. Low-Temperature, Bottom-Up Synthesis of Graphene via a Radical-Coupling Reaction. *J. Am. Chem. Soc.* **2013**, *135*, 9050–9054.
- (19) Liu, J.; Chen, Q.; Xiao, L.; Shang, J.; Zhou, X.; Zhang, Y.; Wang, Y.; Shao, X.; Li, J.; Chen, W.; et al. Lattice-Directed Formation of Covalent and Organometallic Molecular Wires by Terminal Alkynes on Ag Surfaces. *ACS Nano* **2015**, *9*, 6305–6314.
- (20) Mahendar, L.; Ramulu, B. V.; Satyanarayana, G. [Cu]-Catalyzed Direct Coupling of Dibromoalkenes: Synthesis of Symmetrical 1,3-Diynes and Triazoles. *Synth. Commun.* **2017**, *47*, 1151–1158.
- (21) Rao, M. L. N.; Dasgupta, P.; Ramakrishna, B. S.; Murty, V. N. Domino Synthesis of 1,3-Diynes from 1,1-Dibromoalkenes: A Pd-Catalyzed Copper-Free Coupling Method. *Tetrahedron Lett.* **2014**, *55*, 3529–3533.
- (22) Kaldhi, D.; Vodnala, N.; Gujjarappa, R.; Kabi, A. K.; Nayak, S.; Malakar, C. C. Transition-Metal-Free Variant of Glaser- and Cadiot-Chodkiewicz-Type Coupling: Benign Access to Diverse 1,3-Diynes and Related Molecules. *Tetrahedron Lett.* **2020**, *61*, No. 151775.
- (23) Sun, Q.; Tran, B. V.; Cai, L.; Ma, H.; Yu, X.; Yuan, C.; Stöhr, M.; Xu, W. On-Surface Formation of Cumulene by Dehalogenative Homocoupling of Alkenyl *gem*-Dibromides. *Angew. Chem., Int. Ed.* **2017**, *56*, 12165–12169.
- (24) Cai, L.; Kang, F.; Sun, Q.; Gao, W.; Yu, X.; Ma, H.; Yuan, C.; Xu, W. The Stereoselective Formation of *trans*-Cumulene through Dehalogenative Homocoupling of Alkenyl *gem*-Dibromides on Cu(110). *ChemCatChem* **2019**, *11*, 5417–5420.
- (25) Pavliček, N.; Gawel, P.; Kohn, D. R.; Majzik, Z.; Xiong, Y.; Meyer, G.; Anderson, H. L.; Gross, L. Polyyne Formation via Skeletal Rearrangement Induced by Atomic Manipulation. *Nat. Chem.* **2018**, *10*, 853–858.
- (26) Besenbacher, F. Scanning Tunneling Microscopy Studies of Metal Surfaces. *Rep. Prog. Phys.* **1996**, *59*, 1737–1802.
- (27) Laegsgaard, E.; Österlund, L.; Thostrup, P.; Rasmussen, P. B.; Stensgaard, I.; Besenbacher, F. A High-Pressure Scanning Tunneling Microscope. *Rev. Sci. Instrum.* **2001**, *72*, 3537–3542.
- (28) Kresse, G.; Hafner, J. Ab Initio Molecular Dynamics for Open-Shell Transition Metals. *Phys. Rev. B* **1993**, *48*, 13115–13118.
- (29) Kresse, G.; Furthmüller, J. Efficient Iterative Schemes for Ab Initio Total-Energy Calculations Using a Plane-Wave Basis Set. *Phys. Rev. B* **1996**, *54*, 11169–11186.
- (30) Blöchl, P. E. Projector Augmented-Wave Method. *Phys. Rev. B* **1994**, *50*, 17953–17979.
- (31) Kresse, G.; Joubert, D. From Ultrasoft Pseudopotentials to the Projector Augmented-Wave Method. *Phys. Rev. B* **1999**, *59*, 1758–1775.
- (32) Perdew, J. P.; Burke, K.; Ernzerhof, M. Generalized Gradient Approximation Made Simple. *Phys. Rev. Lett.* **1996**, *77*, 3865–3868.
- (33) Grimme, S.; Antony, J.; Ehrlich, S.; Krieg, H. A Consistent and Accurate Ab Initio Parametrization of Density Functional Dispersion Correction (DFT-D) for the 94 Elements H-Pu. *J. Chem. Phys.* **2010**, *132*, No. 154104.
- (34) Tersoff, J.; Hamann, D. R. Theory of the Scanning Tunneling Microscope. *Phys. Rev. B* **1985**, *31*, 805–813.

(35) Henkelman, G.; Uberuaga, B. P.; Jónsson, H. A Climbing Image Nudged Elastic Band Method for Finding Saddle Points and Minimum Energy Paths. *J. Chem. Phys.* **2000**, *113*, 9901–9904.

(36) Kästner, J.; Sherwood, P. Superlinearly Converging Dimer Method for Transition State Search. *J. Chem. Phys.* **2008**, *128*, No. 014106.

(37) Sun, Q.; Cai, L.; Ma, H.; Yuan, C.; Xu, W. Dehalogenative Homocoupling of Terminal Alkynyl Bromides on Au(111): Incorporation of Acetylenic Scaffolding into Surface Nanostructures. *ACS Nano* **2016**, *10*, 7023–7030.

(38) Rabia, A.; Tumino, F.; Milani, A.; Russo, V.; Bassi, A. L.; Achilli, S.; Fratesi, G.; Onida, G.; Manini, N.; Sun, Q.; et al. Scanning Tunneling Microscopy and Raman Spectroscopy of Polymeric sp² Carbon Atomic Wires Synthesized on the Au(111) Surface. *Nanoscale* **2019**, *11*, 18191–18200.

(39) Yang, Z.; Sander, T.; Gebhardt, J.; Schaub, T. A.; Schönamsgruber, J.; Soni, H. R.; Görling, A.; Kivala, M.; Maier, S. Metalated Graphyne-Based Networks as Two-Dimensional Materials: Crystallization, Topological Defects, Delocalized Electronic States, and Site-Specific Doping. *ACS Nano* **2020**, *14*, 16887–16896.